WELDING RESEARCH

SUPPLEMENT TO THE *WELDING JOURNAL*, JANUARY 1988

Sponsored by the American Welding Society and the Welding Research Council

Laser Beam Welding of High-Manganese Stainless Steels—Examination of Alloying Element Loss and Microstructural Changes

Significant changes in the weld metal composition and microstructure have been found during laser beam welding

BY P. A. A. KHAN, T. DEBROY AND S. A. DAVID

ABSTRACT. Alloying element loss and microstructural modifications of high-manganese austenitic stainless steels resulting from laser beam welding were examined. Welds were fabricated using both high- and low-power carbon dioxide lasers. Variables studied were welding speed, laser power and shielding gas flow rate.

Pronounced decrease in the concentration of manganese was observed when specimens were welded at low laser powers. The rate of vaporization of alloying elements such as iron and manganese was found to increase significantly with laser power. However, the decrease in the concentration of manganese was less pronounced when the welds were made at high laser power. The composition change was not significantly influenced by either the welding speed or the shielding gas flow rate. The effective weld pool temperature for vaporization was insensitive to changes in the welding variables. A slight reduction in the concentrations of dissolved oxygen and nitrogen was observed at the surface of the welded specimens. At low laser power, the welded region had a duplex austenitic and ferritic microstructure at low welding speeds and fully austenitic structure at higher welding speeds. However, at high laser powers, the weld microstructure was duplex at all welding speeds.

P. A. A. KHAN and T. DEBROY are with the Department of Materials Science and Engineering, Pennsylvania State University, University Park, Pa. S. A. DAVID is with Oak Ridge National Laboratory, Oak Ridge, Tenn.

KEY WORDS

Laser Beam Welding
Mn Stainless Steels
Weld Metal Changes
Microstructure Changes
Alloy Element Loss
Carbon Dioxide Laser
Weld Pool Temp.
Alloy Vaporization
Welding Speed Effect
Duplex Microstructure

Introduction

Laser beam welding is not an acceptable process for the fabrication of many important engineering alloys that contain one or more volatile elements. The use of a high-power laser beam focused to a very small area leads to a high weld pool temperature and significant vaporization of the relatively more volatile alloying elements. Pronounced loss of alloying elements and the resulting changes in the weld composition during laser beam welding have been documented in the recent past (Refs. 1–3). The loss of alloying elements can result in drastic changes in the microstructure and consequently lead to degradation in both mechanical and corrosion properties. However, no systematic study has been conducted to understand the factors that affect the alloying element vaporization from laser-melted pools. For an alloy of known composition, the rates of vaporization of alloying elements are influenced by the surface area of the molten pool, surface temperature distribution, and other factors that govern the rates of transport of an element from the liquid phase to the

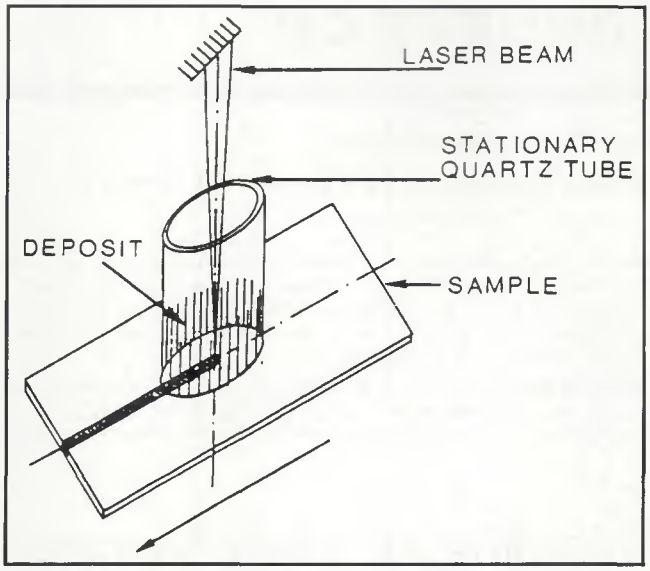

Fig. 1—Experimental setup for collection of vapors

gas/liquid interface and the subsequent transport of the species in the gas phase away from the interface. Although the weld pool temperature is a crucial factor in influencing the alloying element loss, its determination is not straightforward due to the small size of the molten pool and the presence of plasma above the molten pool. One of the major goals of the research reported in this paper was to understand the effects of welding conditions on weld pool temperature, alloying element vaporization rates, and compositional changes due to laser beam welding of AISI 200 series high-manganese stainless steels, using both subkilowatt and multikilowatt carbon dioxide lasers.

In 200 series austenitic stainless steels, nitrogen is added up to 0.25 wt-% to improve strength and to stabilize austenite at room temperature (Refs. 4–6). Since laser beam welding is carried out in a helium or argon atmosphere, mass transfer of impurities such as nitrogen, oxygen and hydrogen can occur between the weld pool and the surrounding environment leading to a change in the concentration of these species in the weld metal. The reduction of nitrogen concentration can contribute to microstructural changes and to a reduction of strength of the welded region. Furthermore, changes in the concentration of hydrogen and other impurities can contribute to the changes in the properties of the material and, in extreme cases, may lead to significant reduction of service life of the fabricated product. The transport of impurities such as oxygen, nitrogen and hydrogen between the molten weld pool and the surroundings is not well understood.

A significant problem in the production of fully austenitic stainless steel welds is their tendency towards hot cracking. To minimize this tendency, the compositions of the weld filler materials are modified to produce small amounts of ferrite in the welded microstructure. Although ferrite has been found to prevent hot cracking effectively (Refs. 7–9), it may also lead to corrosion susceptibility and embrittlement at elevated temperatures. Hence, it would be highly desirable to produce fully austenitic microstructures in stainless steel welds without hot cracking. Rapid solidification conditions encountered during laser beam welding have been found to alter the microstructure of Type 308 stainless steels (Ref. 10). Thus, laser beam welding presents one means by which the normal solidification structure can be significantly altered.

The alloying element loss, distribution of impurities such as oxygen, nitrogen and hydrogen, and microstructural changes that take place during laser beam welding of high-manganese austenitic stainless steels are addressed in this paper.

Experimental Procedures

Samples of high-manganese austenitic stainless steels, namely AISI 201 and 202 steels of approximately 3.5×10^{-2} m (1.4 in.) length, 1.5×10^{-2} m (0.6 in.) width and 0.7 to 2.5×10^{-3} m (0.03 to 0.10 in.) thickness were welded using both subkilowatt and multikilowatt carbon dioxide lasers in continuous wave mode. Samples were placed at the focal point of a 2.54×10^{-2} m (1.1-in.) diameter, 0.127-m focal length Zn-Se lens. The diameter of the focused laser beam was about 0.25×10^{-3} m (0.01 in.). The laser power was in the range of 250 to 4000 W. The welding speeds selected for the experiments were between 3×10^{-3} and 40×10^{-3} m/s (0.12 to 1.6 in./s). The AISI 200 series steels were chosen because of their high concentration of highly volatile manganese and the relative ease in the detection of the decrease in the manganese concentration due to welding. The nominal compositions of AISI 201 and 202 stainless steels are given in Table 1. The welding variables investigated were laser power, welding speed and shielding gas flow rate. All experiments were conducted in an inert atmosphere using helium or argon as the shielding gas. The total rate of alloying element vaporization was determined from the measured values of the loss in sample weight resulting from element vaporization and laser material interaction time. A portion of the vaporized material was collected as condensate inside a both-ends-open, hollow quartz tube mounted coaxial to the laser beam, as shown in Fig. 1. The composition of the condensate was determined by atomic absorption (AA) spectroscopy. The relative rates of vaporization of alloying elements from the weld pool, determined from the analysis of the condensate, were used to estimate the effective weld pool temperature (Ref. 1). Solute loss was determined (Ref. 1) by using electron probe microanalysis (EPMA) technique. A CAMECA IMS-3F ion microprobe was used for the secondary ion mass spectrometry (SIMS) study to determine the concentration profiles of nitrogen, oxygen and hydrogen as a function of depth from the surface of the solidified weld metal. Cs^{133} was used as the primary beam for the sputtering of the samples. Standard metallographic techniques were used for microstructural analysis. The samples were electrolytically etched with a 10% solution of oxalic acid in water using a stainless steel cathode. Microprobe analysis was performed on the samples to generate elemental concentration profiles along selected lines. Spot analyses for manganese, nickel and chromium were performed using wavelength dispersive analysis.

Table 1—Nominal Compositions of AISI 201 and 202 High-Manganese Stainless Steels

Element	Weight-% (201)	Weight-% (202)
C	0.15	0.098
Mn	6.5	7.48
P	0.06	0.032
S	0.03	0.006
Si	1.00	0.47
Ni	4.25	4.72
Cr	17.00	17.85
N	0.07	—
Fe	Balance	Balance

Results and Discussion

Role of Welding Conditions on Alloying Element Loss

Laser Power. For the welding of thin strips of AISI 201 and 202 steels in conduction mode at relatively low laser powers, the changes in concentrations of

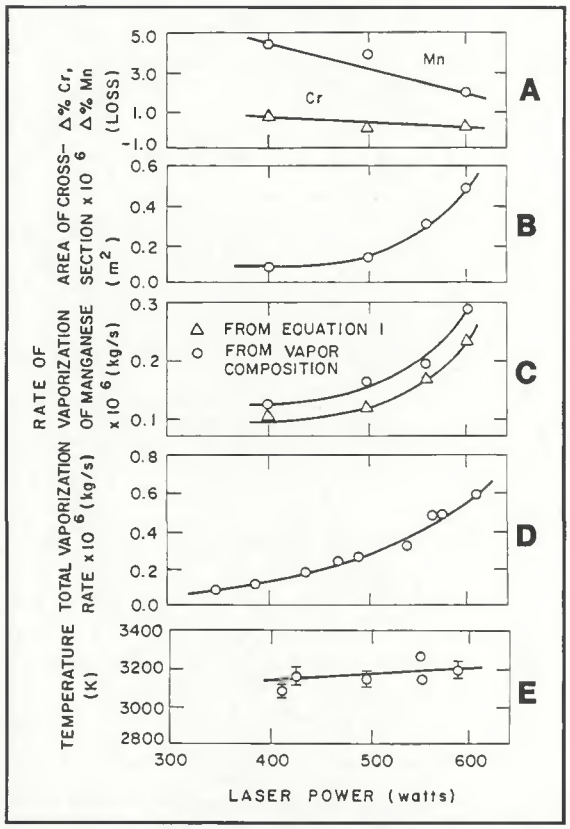

Fig. 2—Effects of laser power on: A—change in weld composition; B—cross-sectional area; C—rate of vaporization of manganese; D—total vaporization rate; E—weld pool temperature in conduction mode of welding. Steel type: AISI 202; welding speed: 3 X 10^{-3} m/s; shielding gas flow rate: 1 X 10^{-4} m^3/s of He; sample thickness: 0.7 X 10^{-3} m

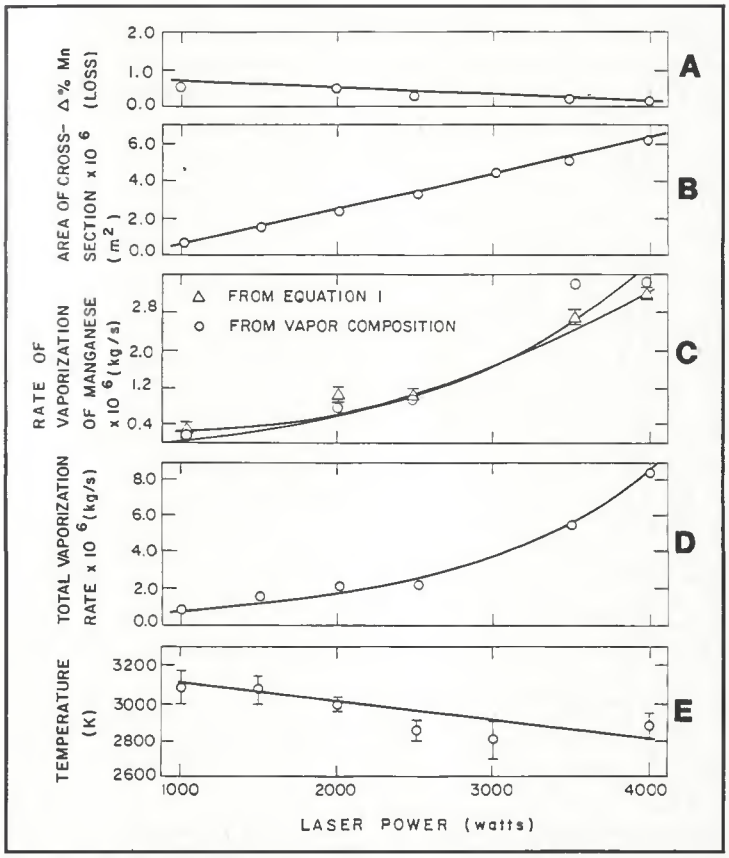

Fig. 3—Effects of laser power on: A—change in weld composition; B—cross-sectional area; C—rate of vaporization of manganese; D—total vaporization rate; E—weld pool temperature in keyhole mode of welding. Steel type: AISI 201; welding speed: 15.24 X 10^{-3} m/s; shielding gas flow rate: 5.5 X 10^{-4} m^3/s of Ar; sample thickness: 2.5 X 10^{-3} m

manganese and chromium as a function of laser power are presented in Fig. 2A. It is observed that a pronounced decrease in the concentration of manganese occurs due to welding. Furthermore, the composition change was most pronounced at relatively low laser powers. A simple mass balance can be performed to understand how the composition change is related to various variables and also to check the mutual consistency of the various types of measurements made. From mass balance, the decrease in the concentration of manganese, Δ%Mn, can be expressed as follows:

$$\Delta\%Mn = 100\ r/Au\rho \qquad (1)$$

where r is the vaporization rate of Mn, A is the cross-sectional area of the molten pool, u is the welding speed, and ρ is the density of steel. It follows from Equation 1 that for a given welding speed, the rate of vaporization of manganese, r, can be estimated from the measured values of Δ%Mn and the area of cross-section of the weld, A. Using the data on Δ%Mn and A presented in Figs. 2A and 2B, respectively, the calculated rate of vaporization of manganese is plotted as a function of laser power in Fig. 2C. In the same figure, the rate of vaporization of manganese, obtained by multiplying the experimentally determined vaporization rate (Fig. 2D) by the fraction of manganese in the vaporized material, is also presented. In view of the uncertainties involved in these experiments, such as possible recondensation of vapors on the sample and the inaccuracies in the determination of weld composition, the agreement between the calculated and the measured vaporization rates of manganese is considered reasonable. The contribution of temperature in the vaporization rate is observed from Fig. 2A, where the effective weld pool temperatures are plotted as a function of laser power. A small increase in weld pool temperature is observed with the increase in laser power due to high input energy.

When the welds were fabricated in the keyhole mode at high laser power using a multikilowatt laser, trends in the changes in composition, cross-sectional area and vaporization rates (Figs. 3A–C) were similar to those obtained in the welding with subkilowatt lasers. Again, although the rate of vaporization increased with power, the change in the composition was less pronounced at high laser power. The increased size of the molten pool in the keyhole mode of welding resulted in less pronounced changes in weld composition. The effective weld pool temperature (Fig. 3E) was not a contributing factor in the increase of the vaporization rate with power.

Welding Speed. The changes in the concentration of manganese as a function of welding speed are presented in Fig. 4A for both low- and high-power laser beam welds. As observed earlier, the change in the composition is more pronounced for the welding at low power. The vaporization rate of manganese was calculated from the data on composition change, cross-sectional area of the weld (Fig. 4B), and the welding speed, using Equation 1. The computed values of the vaporization rate of manganese are presented in Fig. 4C as a function of the welding speed. The vaporization rate of manganese obtained from the weight loss data (Fig. 4D) and the vapor composition is also presented in the same figure. In both cases, it is observed that the vaporization rate increases with the welding speed. At high welding speed, the attenuation of the beam energy by the plasma is less significant, and this

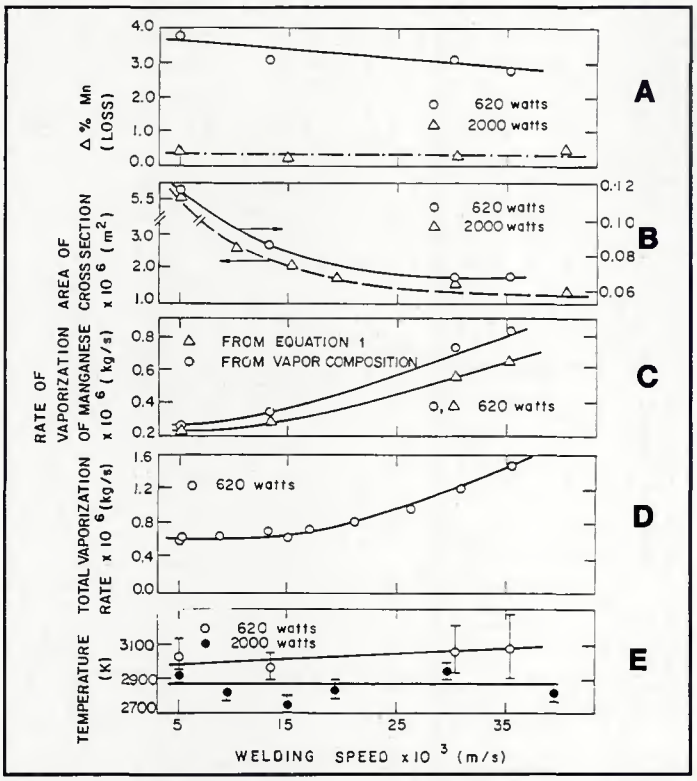

Fig. 4—Effect of welding speed on: A—changes in weld composition; B—cross-sectional area; C—rate of vaporization of manganese; D—total vaporization rate; E—weld pool temperature. AISI 202 stainless steel samples of 0.7 X 10^{-3} thickness were welded at 620 W with a helium (shielding gas) flow rate of 1 X 10^{-4} m^3/s. AISI 201 samples of 2.5 X 10^{-3} thickness were welded at 2000 W with an argon (shielding gas) flow rate of 5.5 X 10^{-4} m^3/s

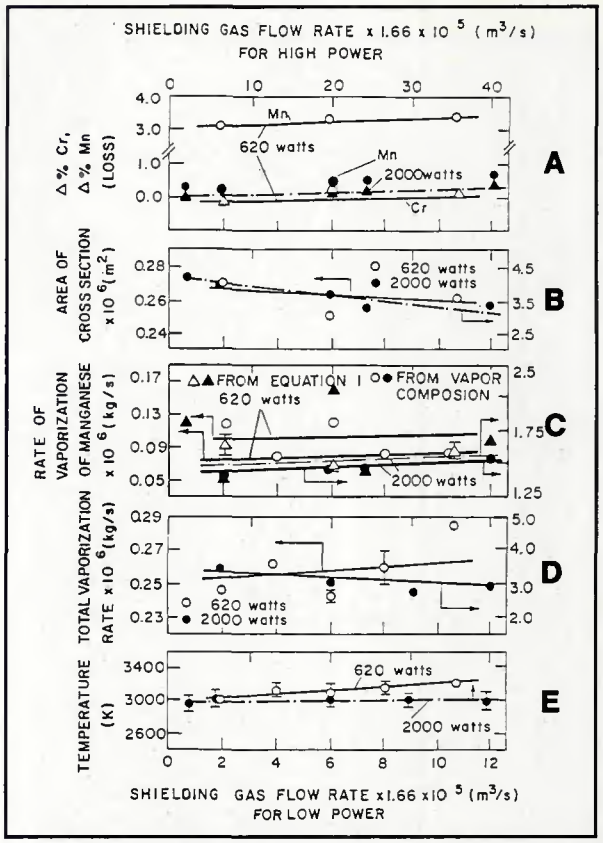

Fig. 5—Effect of shielding gas flow rate on: A—changes in weld composition; B—cross-sectional area; C—rate of vaporization of manganese; D—total vaporization rate; E—weld pool temperature for conduction and keyhole mode of welding. Steel type: AISI 201; welding speed: 3 X 10^{-3} m/s for 1.05 X 10^{-3} m thick samples welded at 620 W using helium as shielding gas, and 15.24 X 10^{-3} m/s for 2.5 X 10^{-3} m thick samples welded at 2000 W using argon as shielding gas

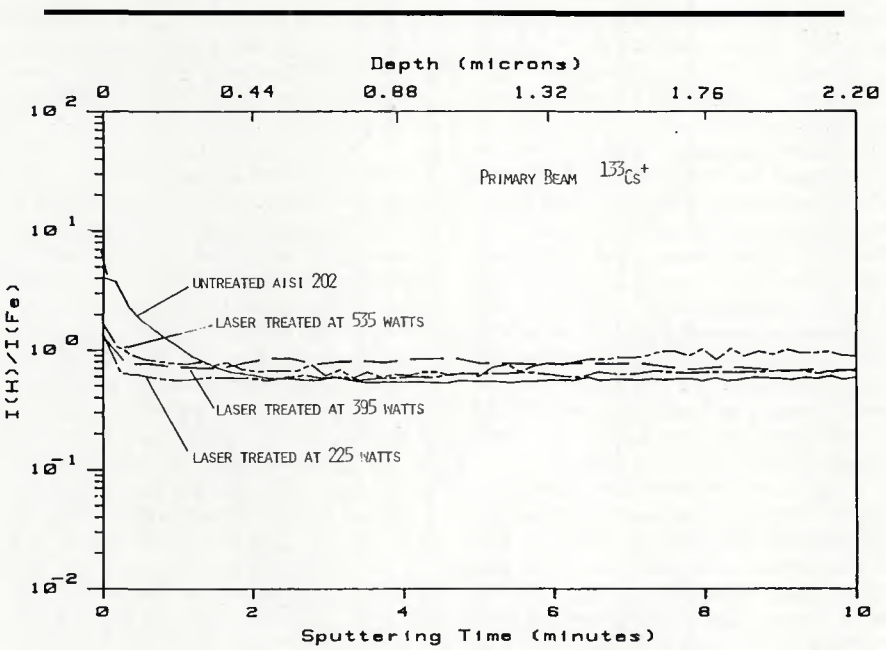

Fig. 6—Relative counts of H/Fe as a function of sputtering time for samples welded at various laser powers. Steel type: AISI 202; primary beam: $^{133}Cs^+$; beam current: 500 nA

results in relatively more exposure of the laser beam on the sample surface. The decreased beam attenuation at high welding speed is also supported by the slight increase in weld pool temperature observed in Fig. 4E. On the whole, weld composition did not change significantly with the welding speed. The increase in the vaporization rate was roughly compensated by the increase in the product of the area of cross-section and the welding speed.

Shielding Gas Flow Rate. The changes in the concentrations of manganese and chromium for the low- and high-power laser beam welds are plotted as a function of shielding gas (He and Ar) flow rate in Fig. 5A. A slight increase in %Mn is observed with the increase in shielding gas flow rate for both high- and low-power welds. It is observed from Fig. 5B that the weld cross-sectional area did not change significantly with the increase in the gas flow rate. The vaporization rate of Mn and the total vaporization rate were found to increase with the increase in the shielding gas flow rate—Figs. 5C and 5D. At high gas flow rates, the

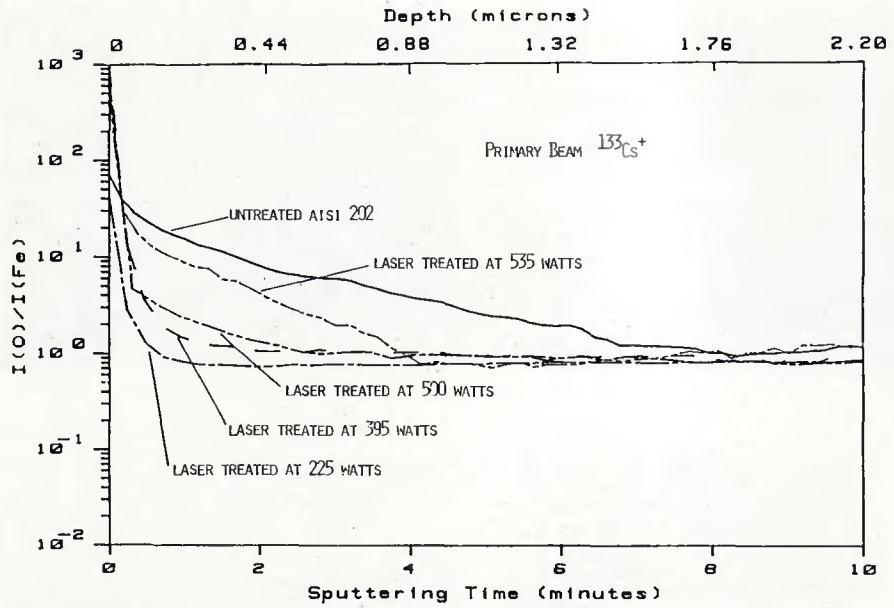

Fig. 7—Relative counts of O/Fe as a function of sputtering time for samples welded at various laser powers. Steel type: AISI 202; primary beam: $^{133}Cs^{+}$; beam current: 500 nA

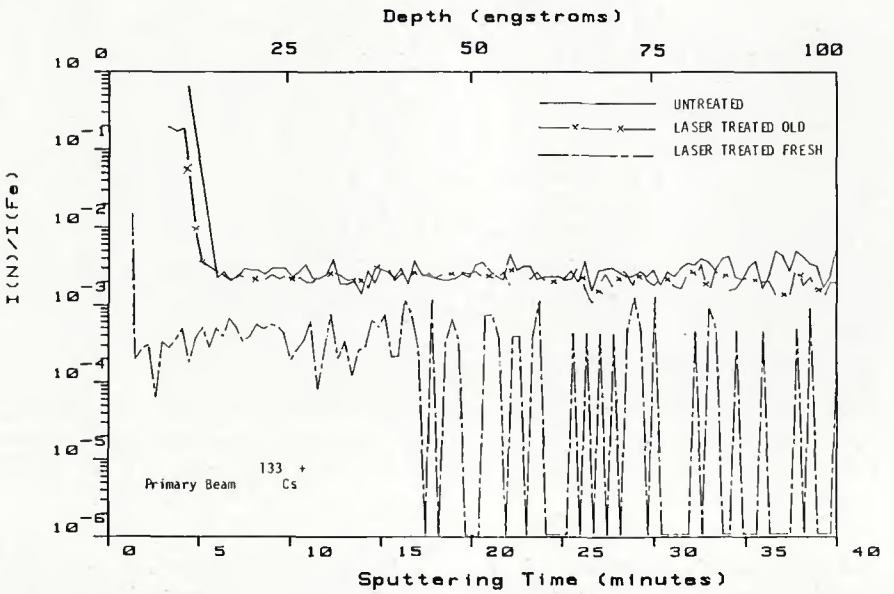

Fig. 8—Relative counts of N/Fe as a function of sputtering time. Steel type: AISI 202; primary beam: $^{133}Cs^{+}$; beam current: 1 nA; laser power: 600 W; welding speed: 3 X 10^{-3} m/s; helium flow rate: 1 X 10^{-4} m^3/s

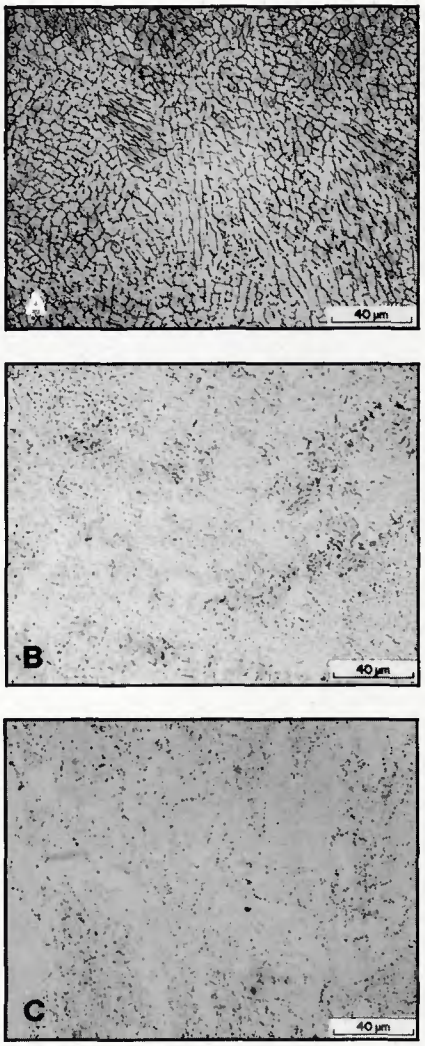

Fig. 9—Microstructures of laser beam welded AISI 200 high-manganese stainless steel observed at different welding speeds. Laser power: 400 W; Welding speed—A—2.2 X 10^{-3} m/s; B—13.2 X 10^{-3} m/s; C—35 X 10^{-3} m/s

plasma covering the laser beam/material interaction site is more effectively flushed away by the shielding gas. This results in enhanced beam absorption and a slight increase in the temperature of the molten pool—Fig. 5E. The shielding gas flow rate does not have a strong influence on the composition change.

Concentration Profiles of Oxygen, Nitrogen and Hydrogen

The concentration of hydrogen, nitrogen and oxygen was analyzed by SIMS since these species can have pronounced influence on the properties of the fabricated product. To compensate for matrix effects, all counts were normalized with respect to iron. The relative concentrations of hydrogen for the base metal and for the samples welded at different laser powers are presented in Fig. 6. It is observed that near the surface of the welded samples, a small drop in the concentration of hydrogen occurred due to welding. In view of the very low activity values of hydrogen in the melt and the low equilibrium partial pressure of hydrogen at the interface, the driving force for the transport of hydrogen from the molten pool to the environment is indeed very small. The normalized concentration profiles of oxygen as a function of depth for samples welded at different laser powers are presented in Fig. 7. It is observed that as the laser power increases, the extent of reduction in oxygen content becomes less pronounced, and at 535 W, the change in the oxygen concentration is practically insignificant. Among the impurities, the concentration of nitrogen is most significant since nitrogen is added to 200 series steels as an austenite stabilizer. A very low beam current of the order of 1 nA was used to sputter the samples at a low rate so that the concentration profiles of nitrogen near the surface layer could be amplified. It can be seen from Fig. 8 that the freshly welded sample has a lower nitrogen concentration at the surface layer than the base metal. Furthermore, when the sample was exposed to air for a period of one year, nitrogen was either

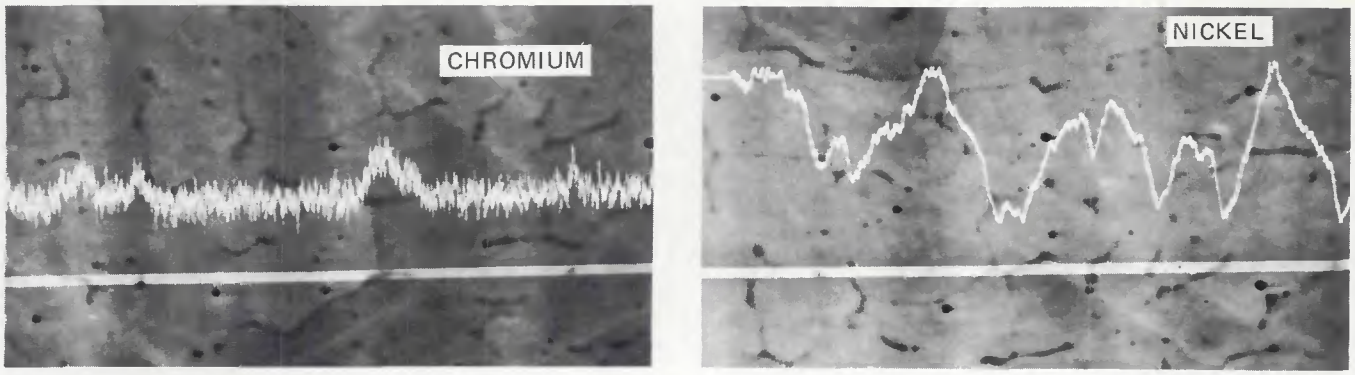

Fig. 10—Chromium and nickel profiles

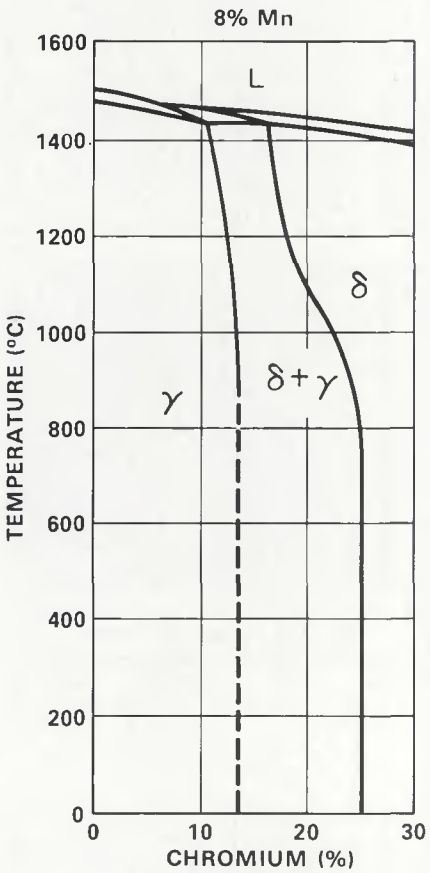

Fig. 11—Vertical section of 8 wt-% Mn in Fe-Cr-Mn system

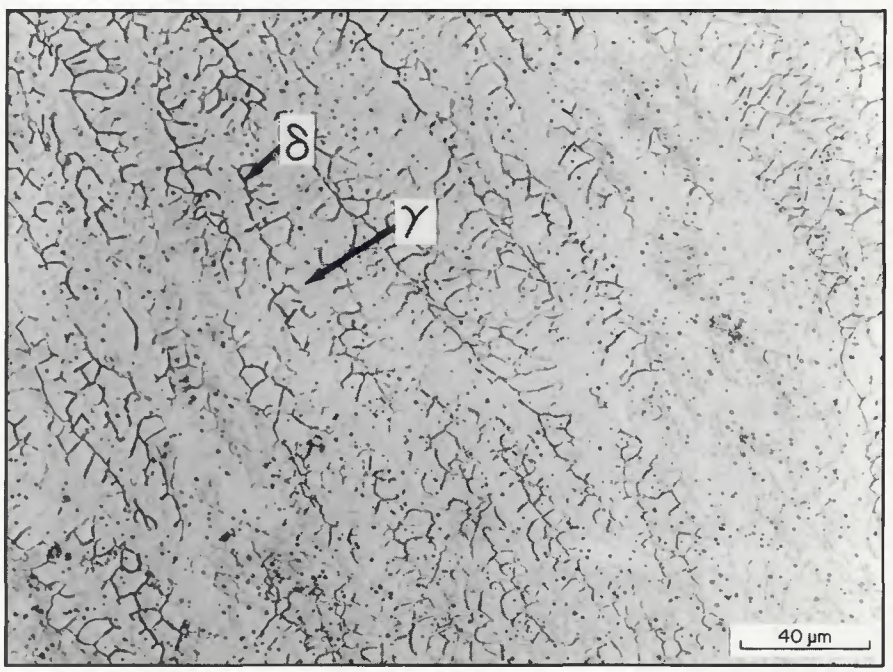

Fig. 12—Microstructure of laser beam welded AISI 201 high-manganese stainless steel. Welding speed: 15 × 10^{-3} m/s; laser power: 4000 W; argon (shielding gas) flow rate: 5.5 × 10^{-4} m^3/s

Table 2—Composition of Different Phases in Weight-%

Welding Condition	Phases	Cr	Mn	Ni
Low Welding Speed (2.2×10^{-3} m/s)	γ	17.0	3.7	4.6
	δ	18.5	3.3	3.5
High Welding Speed (35×10^{-3} m/s)	γ	18.0	6.5	4.2

absorbed from the atmosphere or diffused into the weld metal from the base metal, and its concentration in the weld metal became roughly equal to that in the base metal. When the welding was conducted under a controlled atmosphere of high-purity helium (subkilowatt laser), the bulk nitrogen content of the specimens was found to decrease due to welding. The base metal (AISI 201) was found to contain approximately 0.11 wt-% of nitrogen, whereas the nitrogen content of the weld metal was 0.08 wt-%.

Microstructural Changes

At low laser powers (subkilowatt), the typical microstructures of the laser beam welds are shown in Fig. 9 for various welding speeds. The microstructural features of the welds varied as a function of welding speed. At low speeds of 2.2×10^{-3} m/s (0.09 in./s), the weld contained austenite and ferrite duplex ($\gamma + \delta$) microstructure, with 7 to 8% δ-ferrite in an austenite matrix, as shown in Fig. 9A. As the welding speed increased, the volume-percent of δ-ferrite decreased (Fig. 9B), leading to a fully austenitic microstructure at the high welding speed, as observed in Fig. 9C for a weld made at 35×10^{-3} m/s (1.4 in./s). The presence of δ-ferrite in the weldment was confirmed by a magnetic etching technique described by Gray (Ref. 11). Furthermore, the microprobe analysis results revealed variation in manganese content of the weld as a function of welding speed. For the welds made at low welding speeds and at a power of 400 W, the microprobe results indicated a manganese level of 3.5 wt-%. This compared with the nominal manganese content of the alloy of 7.5 wt-%, indicating a loss of manganese during laser beam welding at

low speeds. The loss was much less significant at high welding speeds. Major elemental compositions of the various constituents present in the microstructures at low and high welding speeds are given in Table 2. The δ-ferrite was found to be slightly enriched in chromium and depleted in nickel, as shown in Table 2 and Fig. 10.

Although the equilibrium structure of 200 series steel is fully austenitic, the indications from the phase diagram, shown in Fig. 11, are that some δ-ferrite is likely to form from liquid as a primary phase during solidification and is retained in the microstructure due to nonequilibrium rapid cooling conditions. This may be further illustrated using the vertical section of 8 wt-% Mn in a Fe-Cr-Mn system (Refs. 12, 13), shown in Fig. 11. Although in the presence of nickel and nitrogen (austenite stabilizers) the $\gamma/\gamma + \delta$ phase boundary is likely to be located further to the right for the Type 202 stainless steel, a low volume-percent of delta ferrite is likely to form from the liquid during solidification and be retained in the microstructure. However, at high welding speeds and relatively high solidification rates (large undercoolings), the weld metal may solidify to 100% austenite. Such observations have been made in other austenitic stainless steels (Refs. 7, 14).

A typical microstructure of the laser beam welds at high laser powers (multikilowatt) is shown in Fig. 12. The microstructures were always duplex with about 6 to 7% δ-ferrite. This was mainly due to a large volume of the weld metal produced at high laser powers and subsequent slow cooling rates experienced by the weld metal.

Conclusions

For the welding of high-manganese austenitic stainless steels at low laser power, the composition of the weld region was significantly different from the composition of the base metal, primarily because of the loss of manganese from the weld pool. At a constant welding speed, the change in the chemical composition was determined by the vaporization rate and the size of the weld pool, with the latter being the dominant factor. Although the rate of vaporization of alloying elements increased with the increase in laser power, the composition change was most pronounced at low laser power because of the small weld pool size. The vaporization rate increased and the weld pool size decreased with the increase in the welding speed. However, the composition change was not sensitive to the changes in the welding speed. At subkilowatt powers and low welding speeds, a duplex ($\gamma + \delta$) microstructure consisting of ferrite and austenite was observed, whereas at high welding speeds, the microstructure was fully austenitic. However, at multikilowatt powers, the microstructure was always duplex ($\gamma + \delta$) at high or low welding speeds. A slight reduction in the concentrations of impurities occurred due to welding.

Acknowledgment

This work was sponsored by the U. S. Department of Energy, Office of Basic Energy Sciences, Division of Materials Science, under grant number DE-FGO2-84FR45158.

References

1. Khan, P. A. A., and DebRoy, T. 1984. *Metallurgical Transactions B,* Vol. 15B, pp. 641-644.

2. Blake, A., and Mazumder, J. 1985. *J. Eng. Ind. Transactions, ASME,* Vol. 107, pp. 275-280.

3. Hettche, L. R., Metzbower, E. A., Ayers, J. D., and Moore, P. G. 1981. *Naval Research Review,* Vol. 28, pp. 4-20.

4. Franks, R., Binder, W. O., and Thompson, J. 1955. *Trans. Soc. Met.,* Vol. 47, pp. 231-266.

5. Pickering, F. B. 1978. *Physical Metallurgy and the Design of Steels,* Applied Science Publishers Limited, London, England.

6. Peckner, D., and Bernstein, I. M. 1977. Chapter 4 in *Handbook of Stainless Steels,* McGraw-Hill Book Company, New York, N. Y.

7. Vitek, J. M., Dasgupta, A., and David, S. A. 1983. *Metallurgical Transactions A,* Vol. 14A, pp. 1833-1841.

8. Borland, J. C., and Younger, R. N. 1960. *British Welding Journal,* Vol. 7, pp. 22-60.

9. Hull, F. C. 1967. *Welding Journal* 46(9):399-s to 409-s.

10. David, S. A. 1981. *Welding Journal* 60(4):63-s to 71-s.

11. Gray, R. J. 1974. Magnetic etching with ferrofluid. *Metallographic Specimen Preparation,* pp. 155-177, Plenum, New York, N. Y.

12. Koster, W. 1933-1937. Die eisenecke des systems eisen-mangan-chrom (the iron corner of the iron-manganese-chromium system). *Archiv. f. d. Eisenhuttenweser,* Vol. 7, pp. 687-688.

13. Kinzel, A. B., and Franks, R. 1940. *Alloys of Iron and Chromium,* Vol. II, p. 277, McGraw-Hill, New York, N. Y.

14. David, S. A., and Vitek, J. M. 1981. Solidification behaviour and microstructural analysis of austenitic stainless steel laser welds. *Lasers in Metallurgy,* conference proceedings of the Metallurgical Society of AIME, pp. 147.